

Electron capture by protons and helium ions from lithium, sodium, and magnesium

R. D. DuBois and L. H. Toburen

Pacific Northwest Laboratories, Battelle Memorial Institute, P.O. Box 999, Richland, Washington 99352

(Received 18 December 1984)

Cross sections for single-electron capture by protons and single- and double-electron capture by helium ions from atomic lithium, sodium, and magnesium targets are presented. The absolute cross sections were measured by using the growth-curve method. Impact energies are in the range 2–100 keV q , where q is the projectile charge state. The present data are compared with previous experimental and theoretical work.

INTRODUCTION

In ion-atom collisions when the projectile velocity is comparable to that of the bound target electrons, electron transfer is an effective method of producing target ionization. Theoretical models used to calculate electron transfer cross sections are generally limited to single-electron systems, e.g., H^+-H or $He^{2+}-H$. Such systems, although attractive theoretically, are difficult to measure experimentally due to the problems associated with atomic hydrogen targets.

Alkali-metal atoms, however, effectively represent quasi-one-electron targets since their single outermost electron is loosely bound with respect to the rest of their electrons. Hence, single-electron models are applicable in describing charge transfer for low-energy proton and alpha-particle impact on alkali-metal targets. These collision systems, in addition, often have practical importance. For example, specific charge-changing collisions with lithium have been suggested as a possible means of obtaining a population inversion capable of lasing in the vacuum ultraviolet or soft x-ray or to be useful in diagnosing properties of the hot plasmas found in present and future thermonuclear fusion reactors.

Because of its suggested applicability as a plasma probe and its few-electron configuration, lithium has been extensively studied. Several theoretical investigations of total one-electron capture have been made for the H^+-Li (Refs. 1–5) and $He^{2+}-Li$ (Refs. 1–3, 6 and 7) systems. These systems are attractive from the theoretical viewpoint since they are effectively “one-electron” systems. Extensive review and tabulation of measured single-electron capture cross sections for H^+-Li collisions have been presented by Barnett *et al.*⁸ for data prior to 1977 and by Nakai *et al.*⁹ for data prior to 1984. Recent measurements have been made for very low energies by Varghese *et al.*¹⁰ and for low to intermediate energies by Aumayr and Winter.¹¹ The recent experimental and theoretical data seem to be in good agreement at lower energies, but at higher energies experiment and theory still differ by a factor of 3 at 100 keV.

For single-electron capture in $He^{2+}-Li$ collisions the atomic-orbital calculations of Fritsch and Lin¹ and molecular-orbital calculations of Sato and Kimura² tend to give similar results but are in conflict with the predic-

tions of Ermolaev and Bransden⁶ who also made atomic orbital calculations. At very low energies the measurements of Varghese *et al.*¹⁰ agree well with the calculations of Fritsch and Lin¹ and Sato and Kimura² but do not extend to sufficiently high energies to merge with the measurements of Murrey *et al.*¹² and McCullough *et al.*¹³ who both indicate a decreasing cross section below 10 keV/amu—similar to the calculations of Ermolaev and Bransden.⁶

Double-electron transfer for $He^{2+}-Li$ collisions is of great interest due to its potential application as a probe of alpha-particle heating in a hot plasma. However, the only theoretical results available are at high energies³ and the only experimental results are those of Murrey *et al.*¹² and McCullough *et al.*¹³ Although both measurements tend to agree, they are subject to large second-order corrections which are necessary owing to competing processes at low energies.

Because of the practical importance of these collision systems and the inconsistencies in the existing data, we have performed measurements of single-electron capture for H^+ and He^{2+} collisions with lithium and for double-electron capture in $He^{2+}-Li$ collisions. In addition, we have measured single-electron transfer for the He^+-Li system where no theoretical work exists. The energy range of the present work is from 2 to 100 keV q where q is the projectile charge state. We thus provide an overlap between the low- and high-energy data that were previously mentioned.

In addition to the Li target, we have measured similar cross sections for Na targets. Again for H^+ and He^{2+} impact, a quasi-one-electron system can be assumed. In the case of proton impact, Kimura *et al.*¹⁴ and Fritsch¹⁵ have performed theoretical calculations while several groups,^{8,16–19} have presented experimental cross sections. The experimental work has been tabulated⁸ as was done for lithium. The agreement between various experiments and between experiment and theory is rather poor. To our knowledge, no previous theoretical or experimental studies of the $He^{2+}-Na$ system have been made; although some previous studies^{8,20–22} of the quasi-one-electron system (He^+-Na) are available.

Finally, we studied the H^+ , He^{2+} , and He^+-Mg systems. Mg is, of course, more complex since it has two loosely bound outer-shell electrons. It has been included

in the present study since it offers additional charge-transfer information for two- and three-electron systems. For Mg targets, very little experimental and no theoretical information exists. Cross sections for H^+ and He^+ have previously been measured^{8,22-24} and tabulated for H^+ impact. But, as was the case for Na, we are aware of no previous studies for He^{2+} impact.

The present results, with an energy range from 2 to 100 kVq, provide charge-transfer cross sections which bridge the low- and high-energy regions. Such data can provide improved consistency tests by comparison to previous experimental and theoretical data in these two energy regions. In addition, by using the same experimental system for different ion species the relative uncertainties for different collision systems should be minimized. This can be quite useful when evaluating the reliability of experimental results and assessing different theoretical treatments.

DATA ACCUMULATION

The experimental apparatus used to measure absolute cross sections for single- and double-electron capture from Li, Na, and Mg is shown schematically in Fig. 1. The charge-analyzed proton and helium ion beams were collimated by two apertures approximately $\frac{1}{8}$ mm in diameter and 25 cm apart. The beams then passed through a 5-cm-long target cell with entrance and exit apertures 1 and 2.5 mm in diameter, respectively.

Immediately after exiting the cell, the beams were charge-state analyzed by an electric field. Following this vertical deflection, a second mutually perpendicular electric field was available for horizontal steering purposes. The post-collision beams were detected approximately 1 m after the target cell by a pair of channel electron multipliers mounted on a precision x - y - z positioner. One of the multipliers could thus be centered on the undeflected neutral component of the post-collision beam while the horizontal and vertical electric fields were adjusted to center the charged component of the beam on the other multiplier. In general the horizontal steering field required was very small, if not zero.

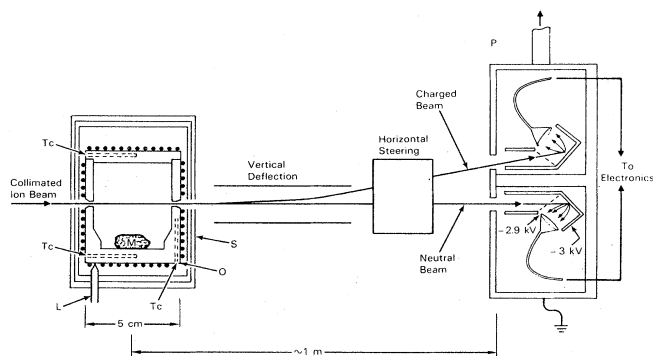


FIG. 1. Schematic of experimental apparatus showing the metal vapor oven, electrostatic beam deflectors and steerers, and the secondary-emission beam particle detection system. O, stainless-steel oven; S, triple heat shield; L, oven support; Tc, oven temperature sensors; P, beam particle detection system.

Cross sections for single- and double-electron capture were measured using the growth-curve method:

$$\sigma_{10} = \frac{-1}{nx} \ln \left[\frac{N^+}{N^+ + N^0} \right] \quad (1)$$

$$\sigma_{21} = \frac{-1}{nx} \ln \left[\frac{N^{2+}}{N^{2+} + N^+ + N^0} \right] \quad (2)$$

$$\sigma_{20} = \frac{1}{nx} \left[\frac{N^0}{N^{2+} + N^+ + N^0} \right] - \left[\frac{1}{nx} \right]^2 \sigma_{21} \sigma_{10} \quad (3)$$

As can be seen from the formulas to measure absolute single-electron transfer cross sections the effective target cell length (x), the absolute target density (n), and the ratio of the post-collision beam components, e.g., $N^+/(N^+ + N^0)$ must be accurately determined. Note that the absolute detection efficiencies of the two multipliers are unimportant. Their relative efficiencies must, however, be the same and independent of ion charge state.

The effective target cell length was determined by adding the geometrical diameter of the cell and the radii of the entrance and exit apertures. The detection efficiencies of the two detectors were investigated in several ways. In an initial configuration, the ion beams impinged directly on the multiplier cones. By applying a large negative voltage to the cones, ions were detected only with they impinged deep in the throats of the multipliers. Scanning the detectors across the beams for low impact energies showed that the post-collision beams were less than 1 mm in diameter even at low energies where the collisional beam scattering should be the largest. For a slightly positive cone bias (the normal situation used in the experiment) ions were detected with constant efficiency across the entire cone. Thus the solid angles subtended by the multipliers were large enough to detect all scattered ions leaving the collision volume. The solid angle subtended by the exit aperture of the target cell is larger than that subtended by the detector; hence no loss of ion signal due to aperture restriction or insufficient detector solid angle is anticipated. Next, under stable operating conditions, the ratio $N^+/(N^+ + N^0)$ was measured and then the deflection field was reversed and the detectors repositioned so as to interchange the charged and uncharged beam detectors. The ratio was then remeasured and confirmed to be unchanged. Thus both multipliers were equally sensitive to charged and uncharged ions.

Later, the detectors were redesigned to operate in a secondary-emission mode as described by Rinn *et al.*²⁵ Again, reversing the incident beams to the detectors demonstrated similar detection efficiency for charged and uncharged beams. In addition, the absolute detection efficiencies were measured at higher impact energies for neutral, singly, and doubly charged ions. This was done by comparing the counting rates for the secondary-emission detectors with those obtained using a surface-barrier detector. It was found that, within the experimental uncertainty of approximately 5%, both detectors had unit efficiency.

Using this efficiency and cell length information, single-electron transfer cross sections for H^+ -He, N_2 , and

Ar collisions were measured. To do this, the target cell cover was replaced with one through which target gases could be injected and the absolute target densities measured by means of a capacitance manometer. The absolute cross sections measured between 5 and 100 keV were in excellent agreement with tabulated values.⁸ These results reaffirmed our confidence in the experimental technique and that the target length and detection efficiencies used were accurate.

For metal vapor targets the primary difficulty in absolute cross-section measurements lies in the accurate determination of the absolute target density. To determine the density, the temperature T of the oven and the metal sample must be well known and then related to the vapor pressure through $n = 3.6 \times 10^{13} P (T_0/T) \text{ cm}^{-3}$ where T_0 is the absolute temperature 273.16 and P is the pressure in mTorr obtained from the vapor pressure curves of Hultgren *et al.*²⁶ and Nesmeyanov.²⁷ Temperature uncertainties of approximately $\pm 1^\circ\text{C}$ relate to pressure, and hence cross-section, uncertainties of nearly $\pm 8\%$.

To ensure and test for uniformity in oven temperature, the stainless-steel oven was encased in a triple-layered stainless-steel heat shield. Heating was done by a resistive heating element soldered directly to the oven. Temperature probes were inserted in 2-cm-deep holes drilled into the oven base, and oven side wall, and the oven top. Initially, before loading the oven with metal, platinum resistance thermometers in ceramic casings were used as temperature probes. These high resistance devices have the advantage that junctions with dissimilar metal lead wires do not require compensation as is the case with thermocouple temperature probes. Temperature variations were found to be less than 1°C between the oven base and side wall as the temperature was increased and decreased slowly through the range used for data taking. In addition, after loading the oven with metal, it was shown that the measured cross sections were essentially unaffected by the temperature of the independently heated oven top when its temperature was increased and decreased corresponding to vapor pressure changes of a factor of 2. Thus the oven base temperature where the metal is located determines the vapor pressure of the target.

These high-resistance temperature-measuring devices were later abandoned in favor of thermocouples after it was found that their temperature characteristics changed after being subjected to a lithium vapor environment. This is believed to be due to lithium absorption into the ceramic casing. The change in the calibration was confirmed by comparing a "contaminated" platinum thermometer with a chromel-alumel thermocouple and also comparing both temperature-measuring devices with known temperature sources such as liquid nitrogen, ice-water, and boiling water. In addition, by observing the change of oven temperature as a function of time while slowly raising the temperature, the melting point of lithium could be observed as a change in slope. This provided an absolute temperature point near normal operating conditions.

After replacing the oven base temperature sensor with a chromel-alumel thermocouple referenced to the chamber walls, cross-section measurements agreed with earlier

measurements made using the recalibrated platinum thermometer. These resulting cross sections have temperature-associated errors of approximately $\pm 10\%$.

In a typical experimental run the oven was loaded with a high-purity metal. After pump down the oven temperature was cycled several times in order to outgas the target cell and break any oxide layers that had formed during the loading process. The temperature was then adjusted to a value that corresponded to a target vapor pressure of 10^{-6} Torr or less. Background chamber pressures at this time were typically 2×10^{-7} Torr or less.

The experimental apparatus and ion beam were then adjusted until a neutralized beam component less than approximately 1% of the direct beam intensity was achieved. Since pulse counting methods were used, beam intensities less than 10^{-15} A were used. The post-collision beams were centered on their respective detectors as previously described.

At that point the oven temperature was slowly increased to provide target pressures ranging from approximately 10^{-5} Torr to $(1-2) \times 10^{-3}$ Torr. During this time the fractional beam neutralization, e.g., $N^+/(N^+ + N^0)$ along with the oven temperature were recorded. This process was repeated as the oven cooled down to its original value. Plots of $-\ln[N^+/(N^+ + N^0)]$ versus the target pressure P were made and fitted to formula (1). The cross section calculated for increasing and decreasing temperatures were found to agree within approximately 10% implying that there is no inertial delay in the oven temperature measurement.

In the case of He^{2+} impact, the He^{2+} , He^+ , and He^0 beams could not all be recorded simultaneously. Thus the deflection field was varied in order to measure the He^{2+} and He^0 components and then the He^+ and He^0 components. This process was repeated several times in order to ensure that the oven temperature and beam intensity remained stable during the measurements. For He^{2+} impact, formula (3) was used in order to correct for the two-step process $\sigma_{21}\sigma_{10}$ contributing to the double-electron transfer cross section.

The absolute cross sections determined are believed to be accurate to approximately $\pm 15\%$ with most of the uncertainty due to the absolute target densities measured. The relative uncertainties between cross sections for different projectiles are considerably less than the uncertainties in the absolute value with the precision being determined primarily by instrument reproducibility which was normally about $\pm 5\%$. This applies also, but to a lesser extent, to the relative uncertainties between cross sections measured for various targets since any errors in the oven temperature scale would be expressed in the same manner for each metal vapor target. Cross-section uncertainties recorded in the following tables are representative experimental reproducibilities only and are, in general, larger for data obtained at the extremes of the energy range. Also, note that the double-charge-transfer cross section σ_{20} is subject to larger uncertainties at low energies. This is due to the large second-order corrections that must be applied to the raw data [second term in formula (2)]. In this case we have assigned an additional uncertainty resulting from a $\pm 10\%$ uncertainty in both σ_{21} and σ_{10} . The $\pm 10\%$ un-

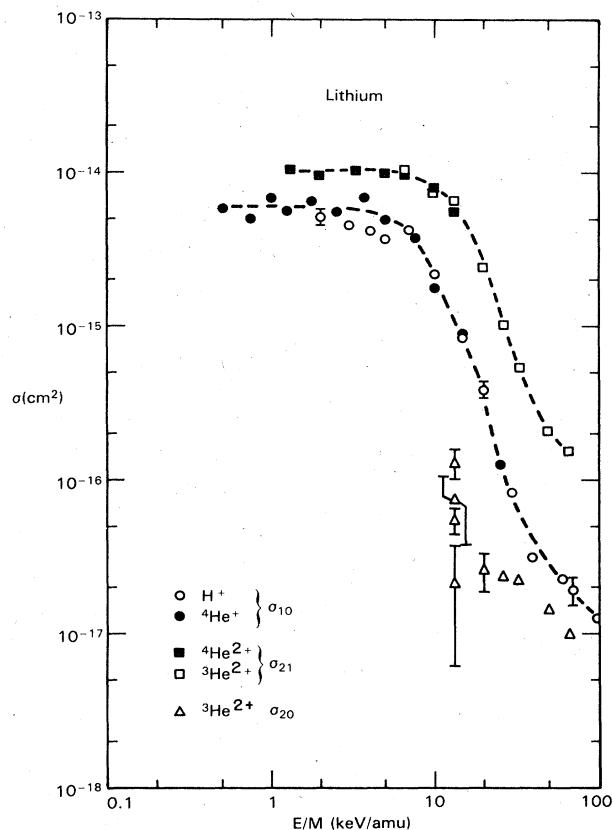


FIG. 2. Single- and double-electron transfer cross sections for proton and helium-ion impact on lithium. Error bars for σ_{20} as described in text.

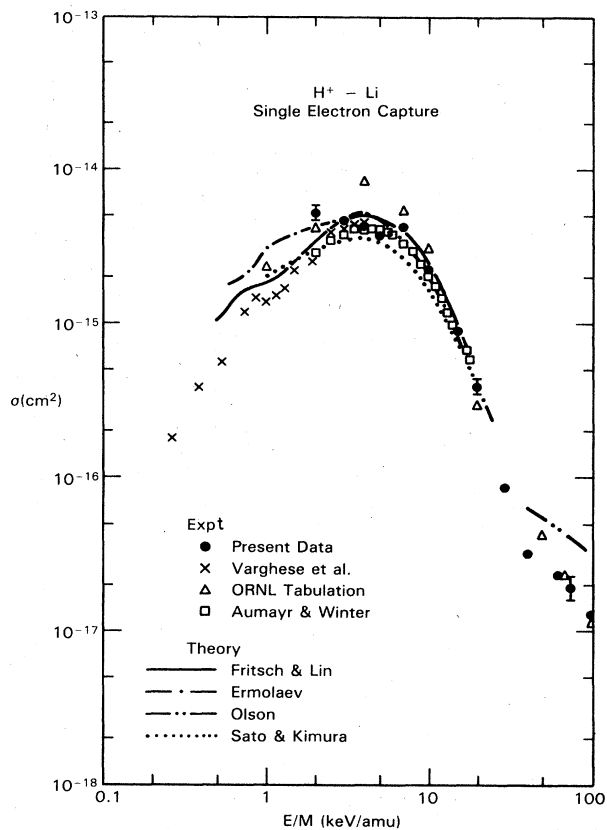


FIG. 3. H^+ -Li single-electron transfer cross sections. Experiment: \bullet , present data; \times , Ref. 10; Δ , tabulated values from Ref. 8; \square , Ref. 11. Theory: —, Ref. 1; - - -, Ref. 4; - · - ·, Ref. 3; · · ·, Ref. 2.

TABLE I. Cross sections for electron transfer in proton and helium ion collisions with lithium atoms. Cross sections are in units of 10^{-16} cm^2 . Tabulated errors represent reproducibility only; absolute accuracy is estimated as $\pm 15\%$. In the case of σ_{20} the uncertainties shown also include contributions from the estimated error in the two-step process ($\sigma_{21}\sigma_{10}$) as explained in the text.

Energy (keV)	σ_{10}		σ_{21}		σ_{20}
	H^+	${}^4\text{He}^+$	${}^3\text{He}^{2+}$	${}^3\text{He}^{2+}$	
2	52.4 \pm 5.9	58.3			
3	46.5	50.4			
4	42.7	68.4	103.3		
5	37.2	57.0			
6			95.1		
7	43.5	66.6			
10	22.1 \pm 0.4	57.1	114 \pm 10		
15	8.86	71.7	97.4		
20	3.84 \pm 0.38	49.7 \pm 2.5	99.3 \pm 2.8		
30	0.857	38.8	75.1 \pm 0.4		0.76 \pm 0.2 ^a
40	0.319	18.1	59.6 \pm 4.9		
60	0.230	8.93	23.3 \pm 0.1		0.251 \pm 0.07
70	0.194 \pm 0.040				
80	0.190	4.24	9.94		0.230
100	0.129	1.30	5.39		0.216
150			2.03		0.139
200			1.50		0.0959

^aValue is weighted average of the data shown in Fig. 2.

certainty was chosen between the maximum *absolute* uncertainty and the minimum *reproducibility* uncertainty as given above. It thus provides an indication as to the reliability in correcting for the two-step process.

RESULTS

Lithium

Results for the lithium target are shown in Fig. 2 and tabulated in Table I. The results, tabulated as a function of impact energy, are graphed versus projectile energy/mass (E/amu). Previously it has been observed²⁴ that equal-velocity H^+ and D^+ ions have the same charge-transfer cross section. For the present data, equal-velocity H^+ and He^+ have nearly the same cross sections, which may indicate the effectiveness of screening by the He^+ electron. The dashed curves through the data serve merely to guide the eye.

The measured double-electron capture cross sections for He^{2+} impact are shown at the bottom of the figure. At the highest energies measured, the reproducibility of the data was better than the size of the data points shown. However, at the lowest energy the reproducibility is poor. In addition, corrections for the two-step process $\sigma_{21}\sigma_{10}$ are extremely large. The error bars shown are calculated

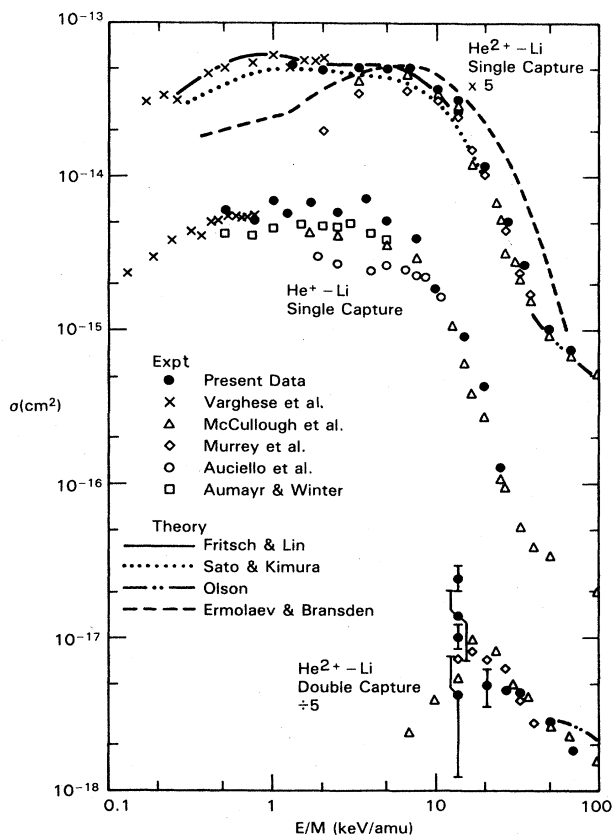


FIG. 4. Single- and double-electron capture cross sections for helium-ion collisions with lithium. Experiment: ●, present data; ×, Ref. 10; △, Ref. 13; ◇, Ref. 12; ○, Ref. 28; □, Ref. 11. Theory: —, Ref. 1; ···, Ref. 2; - · -, Ref. 3; ---, Ref. 4.

using the assumption that the cross sections contributing to this two-step process are each uncertain by $\pm 10\%$. The two-step contribution to σ_{20} , and hence the associated error, increase dramatically for lower impact energies and completely dominate the observed double-electron transfer signal. Thus we feel that the present σ_{20} data are reliable only for energies above 20 keV/amu.

In Figs. 3 and 4 we compare our present measurements with previous experimental and theoretical results. For proton impact, except for our lowest energy point, we agree well with the recent measurements of Varghese *et al.*¹⁰ and Aumayr and Winter¹¹ which merge smoothly into the cross sections tabulated by Barnett *et al.*⁸ at energies greater than about 15 keV. The theoretical calculations of Fritsch and Lin¹ give the best overall agreement with the data. At higher energies we have better agreement with the tabulated cross sections⁸ than the calculations of Olson.³

For He ion impact, Fig. 4, we again agree well with the measurements of Varghese *et al.*¹⁰ and the calculations of Fritsch and Lin.¹ However, the present cross sections for σ_{21} and σ_{10} are larger than those measured previously between 2 and 10 keV/u. Again we note that any uncertainties in these cross sections can drastically effect the double-electron capture cross section at low energies. For example, formula (3) indicates that an underestimation of both σ_{21} and σ_{10} will result in an overestimation of σ_{20} .

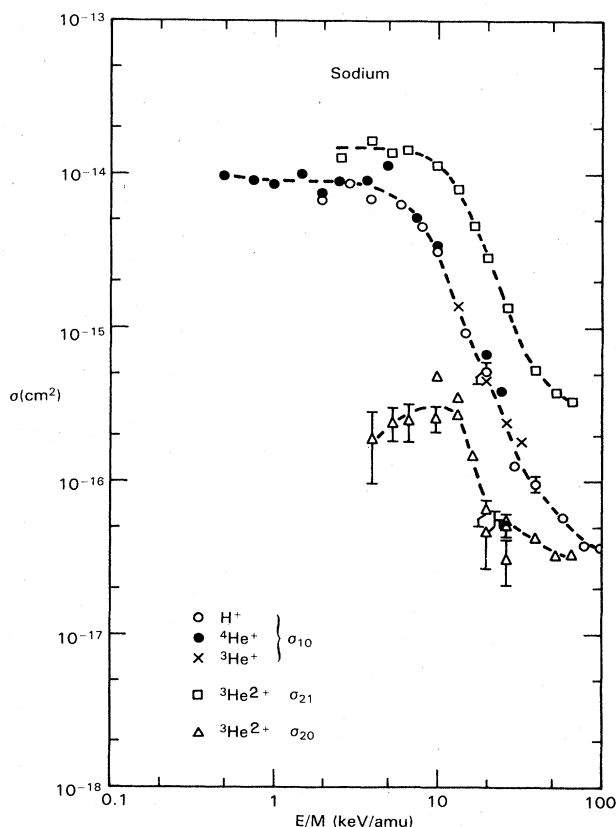


FIG. 5. Single- and double-electron transfer cross sections for proton and helium-ion impact on sodium. Error bars for σ_{20} as described in text.

Our double capture cross sections shown at the bottom of the figure agree well with previous measurements at higher energies.

SODIUM

In Fig. 5 we show our current measurements of single- and double-electron transfer cross sections for H^+ , He^+ , and He^{2+} impact on sodium. Numerical values of the cross sections are listed in Table II. Again we have plotted the data versus the energy/mass as we had done for lithium; and again we note the single charge-transfer cross sections for equal-velocity H^+ and He^+ impact are approximately equal throughout the entire energy range. Also, the single-electron transfer cross sections have approximately a constant value below ~ 5 keV/amu.

The double-electron transfer cross section, however, clearly peaks near 10 keV/amu. This is similar to the lithium measurements of McCullough *et al.*¹³ (see Fig. 4). For sodium the double charge transfer cross sections are about a factor of 3 larger than those measured for lithium in contrast to the single charge transfer cross sections which are only about 30% larger. Because of this the second-order corrections to the double charge transfer cross sections in sodium are considerably smaller than they were in the case of lithium. As before, the error bars shown for σ_{20} represent an uncertainty of $\pm 10\%$ in each of the cross sections contributing to this two-step contribution.

In Fig. 6 we compare our present measurements with those of previous investigations. For proton impact, we find our results are in reasonable agreement with the tabulated values of Barnett *et al.*⁸ above 10 keV/amu and with Anderson *et al.*¹⁷ for all energies, but disagree with

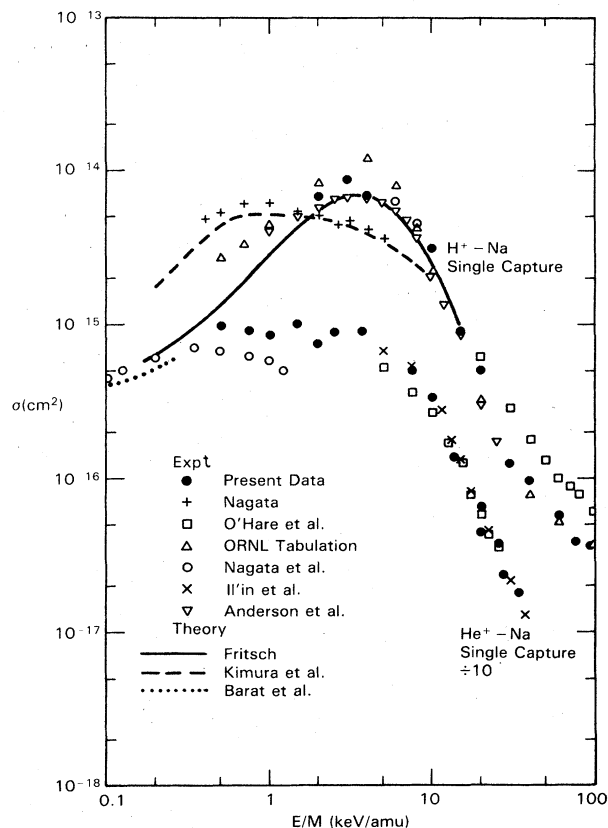


FIG. 6. H^+ , He^+ -Na single-electron transfer cross sections. Experiment: \bullet , present data; $+$, Ref. 16; \square , Ref. 18; \triangle , tabulated values from Ref. 8; \circ , Ref. 21; \times , Ref. 22; ∇ , Ref. 17. Theory: —, Ref. 15; — —, Ref. 14; \cdots , Ref. 20.

TABLE II. Cross sections for electron transfer in proton and helium-ion collisions with sodium atoms. Cross sections are in units of 10^{-16} cm². Tabulated errors represent reproducibility only; accuracy in the absolute value is estimated at $\pm 15\%$. In the case of σ_{20} the uncertainties shown also include contributions from the estimated error in the two-step process ($\sigma_{21}\sigma_{10}$) as explained in the text.

Energy (keV)	H^+	$\sigma_{10} \text{ } ^4He^+$	$^3He^+$	$\sigma_{21} \text{ } ^3He^{2+}$	$\sigma_{20} \text{ } ^3He^{2+}$
2	66.4	98.2			
3	85.2	90.4			
4	68.9	85.2			
6	62.1	98.4			
8	45.4	75.9		124.6	
10	30.8	89.6			
12				163.5	1.88 ± 0.094
15	9.37	91.5 ± 1.8			
16				137.4	2.39 ± 0.58
20	5.03 ± 0.8	115.2		141.7	3.7 ± 1.1^a
30	1.25 ± 0.08	50.7 ± 3.9		113.3 ± 2	3.06 ± 0.40^a
40	0.966 ± 0.1	33.8 ± 0.7	13.6 ± 0.5	79.6 ± 3	
50				45.9	1.41 ± 0.10
60	0.575		4.46	28.1 ± 0.6	0.558 ± 0.075^a
80	0.372 ± 0.048	6.70	2.34	13.6 ± 1.6	0.487 ± 0.062^a
100	0.363 ± 0.010	3.86	1.85		
120				5.22	0.416 ± 0.011
160				3.83 ± 0.10	0.315 ± 0.012
200				3.39	0.324 ± 0.012

^aValues are weighted averages of the data shown in Fig. 5.

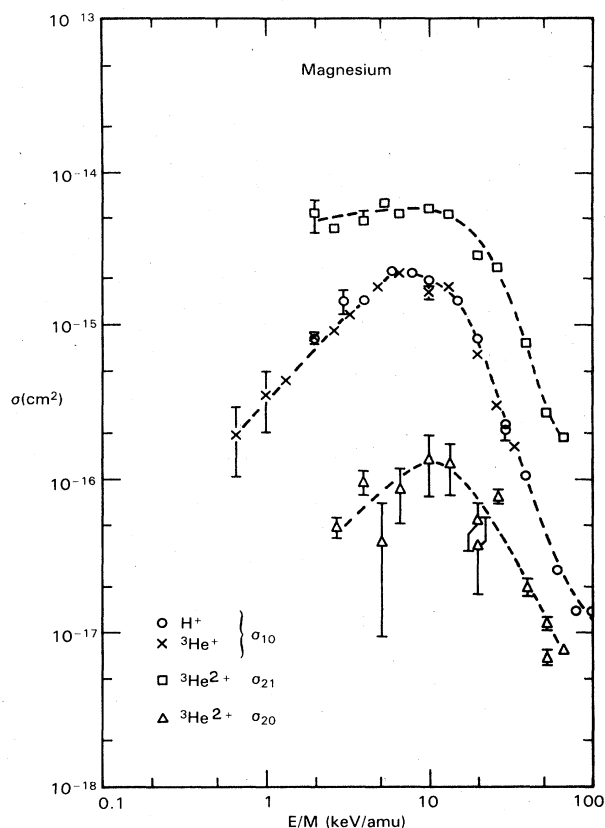


FIG. 7. Single- and double-electron transfer cross sections for proton and helium-ion impact on magnesium. Error bars for σ_{20} as described in text.

the measurements of Nagata¹⁶ and O'Hare *et al.*¹⁸ With respect to theory, our data disagree with the calculations of Kimera *et al.*,¹⁴ which tend to follow the measurements of Nagata¹⁶ but are in reasonable agreement with recent calculations of Fritsch.¹⁵

For He⁺ impact, at higher energies the present data agree nicely with those of Il'in *et al.*²² and O'Hare *et al.*¹⁸ But we again disagree with the measurements of Nagata *et al.*²¹ The disagreement between the data of Nagata *et al.* and our results would be removed for both He⁺ and He²⁺ impact by a simple renormalization amounting to increasing the Nagata data by about 25%. This would, however, increase the disagreement between the He²⁺ data of Nagata *et al.* and other workers for energies below about 2 keV/amu which leaves a considerable question as to the cross sections for these very low energies. The only available theoretical work for He⁺ is that of Barat *et al.*²⁰ which is for much lower energies and thus cannot be tested with the present data.

MAGNESIUM

Magnesium provides a slightly different situation than lithium or sodium since in this case the outer shell contains two loosely bound electrons. It thus provides a challenging extension for existing theoretical treatments. Results for magnesium are shown in Fig. 7 and are listed in Table III. Again the σ_{10} curves for equal velocity H⁺ and He⁺ impact coincide. Unlike the results for lithium and sodium targets, the σ_{10} cross sections are not constant below 10 keV/amu but reach a maximum and then decrease. Results for σ_{21} are, on the other hand, nearly constant below 10 keV/amu as was the case for the other two targets.

TABLE III. Cross sections for electron transfer in proton and helium-ion collisions with magnesium atoms. Cross sections are in units of 10^{-16} cm². Tabulated errors represent reproducibility only; accuracy in the absolute values is estimated as $\pm 15\%$. In the case of σ_{20} the uncertainties shown also include contributions from the estimated error in the two-step process ($\sigma_{21}\sigma_{10}$) as explained in the text.

Energy (keV)	H ⁺	σ_{10}	³ He ⁺	σ_{21} ³ He ²⁺	σ_{20} ³ He ²⁺
2	8.14±0.66		1.95±0.94		
3	14.2±2.5		3.50±1.43		
4	14.5		4.29	39.5±30.7	
6	22.7		8.12	54.0±14.9	
8	21.7		9.23	43.7	0.488±0.083
10	19.5		11.9		
12				48.3	0.957±0.177
15	14.5		18.1		
16				61.0	0.398±0.304
20	8.10±0.3		22.9	53.9	0.836±0.336
30	2.00±0.25		16.0±1.7	57.6	1.32±0.55
40	1.05		1.76	52.5	1.23±0.46
60	0.248		6.35	27.6±2.4	0.447±0.053 ^a
80	0.137±0.015		2.98±0.03	23.1	0.798±0.059
100	0.135		1.61		
120				7.50	0.196±0.023
160				2.70±0.02	0.092±0.016 ^a
200				1.87	0.0754±0.0017

^aValues are weighted averages of the data shown in Fig. 7.

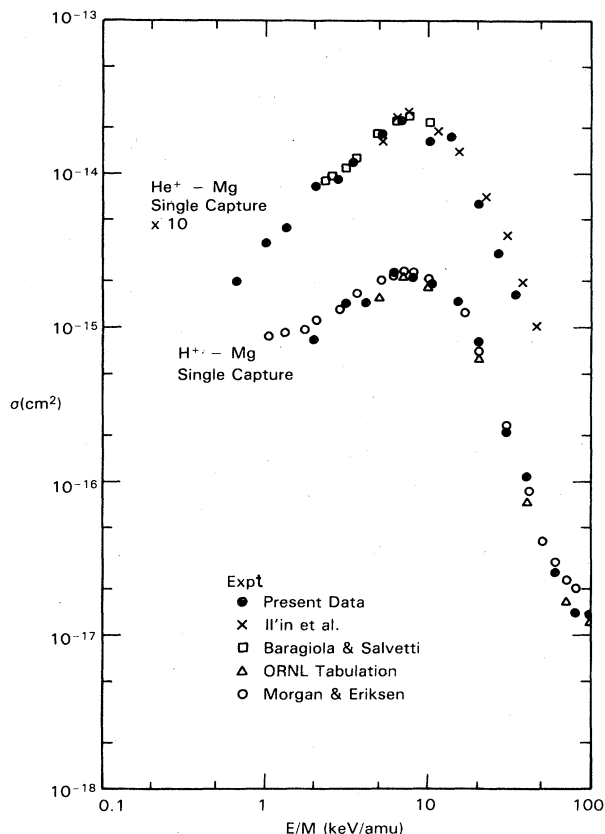


FIG. 8. H^+ , He^+ -Mg single-electron transfer cross sections. Experiment: ●, present data; ×, Ref. 22; □, Ref. 23; △, tabulated values from Ref. 8; ○, Ref. 24.

The double charge-transfer cross section is again peaked as was seen for lithium and sodium. It is interesting to note that both the single and double charge-transfer cross sections for magnesium are smaller than they were for sodium even though magnesium has two loosely bound electrons and sodium has but one. This no doubt confirms the assertion that simple energetics are insufficient to predict even relative cross sections in this energy region and supports the need for greater theoretical activity which encompass the full molecular nature of these collisions.

In Fig. 8 we compare our present results with previously measured cross sections and find good agreement for both H^+ and He^+ impact. No previous data is known to exist for He^{2+} impact. Note that the low-energy proton impact data of Morgan and Erikson²⁴ are progressively larger than those for equal-velocity He^+ impact as the ion energy decreases. This is in conflict with our observations that the cross sections for equal-velocity H^+ and He^+ impact are equal.

CONCLUSIONS

We have presented measurements of absolute single- and double-electron transfer cross sections for proton and helium-ion impact on lithium, sodium, and magnesium targets. The cross sections for simple electron capture when combined with previous experimental and theoretical work have, in most cases, produced unambiguous curves over a broad energy range. Double-electron capture cross sections for He^{2+} impact were obtained from measured transmitted beam fractions and corrections for multi-step single capture processes measured in the same apparatus. The measured double-electron capture cross sections were shown to be extremely sensitive to the cross sections contributing to the two-step electron transfer process. The peaked behavior of σ_{20} for lithium could not be confirmed but was shown to be similar to that clearly observed for He^{2+} -Na and Mg collisions which were measured for the first time. Double-electron capture was found to be approximately a factor of 3 times larger for sodium than for lithium whereas the single-electron capture cross sections were only about 30% larger for sodium than for lithium. In contrast to sodium, magnesium, which has two loosely bound electrons, produced a two-electron transfer cross section σ_{20} which was less than a factor of 2 larger than for lithium. Additional theoretical work will be required to explain these observations.

ACKNOWLEDGMENTS

This paper is based on work supported by U.S. Department of Energy (Division of Magnetic Fusion Energy), under Contract No. DE-AC06-76RL01830.

¹W. Fritsch and C. D. Lin, *J. Phys. B* **16**, 1595 (1983).

²H. Sato and M. Kimura, *Phys. Lett.* **96A**, 286 (1983).

³R. E. Olson, *J. Phys. B* **15**, L163 (1982).

⁴A. M. Ermolaev, *J. Phys. B* **17**, 1069 (1984).

⁵R. J. Allan, A. S. Dickinson, and R. McCarroll, *J. Phys. B* **16**, 467 (1983).

⁶A. M. Ermolaev and B. H. Bransden, *J. Phys. B* **17**, 1083 (1984).

⁷M. T. Stollberg and H.-W. Lee, *Phys. Rev. A* **29**, 2448 (1984).

⁸C. F. Barnett, J. A. Ray, E. Ricci, M. I. Wilker, E. W. McDaniel, E. W. Thomas, and H. B. Gilbody, Oak Ridge National Laboratory Report No. ORNL-5206, Vol. I, 1977 (unpublished), tabulates data prior to 1977.

⁹Y. Nakai, T. Shirai, M. Sataka, and T. Sugiura, Japan Atomic Energy Research Institute Report No. JAERI-M-84-169, 1984 (unpublished), tabulates data prior to 1984.

¹⁰S. L. Varghese, W. Waggoner, and C. L. Cocke, *Phys. Rev. A* **29**, 2453 (1984).

¹¹F. Aumayr and H. Winter, *Phys. Rev. A* **31**, 67 (1985).

¹²G. A. Murray, J. Stone, M. Mayo, and T. J. Morgan, *Phys. Rev. A* **25**, 1805 (1982).

¹³R. W. McCullough, T. V. Goffe, M. B. Shah, M. Lennon, and H. B. Gilbody, *J. Phys. B* **15**, 111 (1982).

¹⁴M. Kimura, R. E. Olson, and J. Pascale, *Phys. Rev. A* **26**, 1138 (1982); **26**, 3113 (1982).

¹⁵W. Fritsch, *Phys. Rev. A* **30**, 1135 (1984).

- ¹⁶T. Nagata, *J. Phys. Soc. Jpn.* **48**, 2068 (1980).
- ¹⁷C. J. Anderson, A. M. Howald, and L. W. Anderson, *Nucl. Instrum. Methods* **165**, 583 (1979).
- ¹⁸B. G. O'Hare, R. W. McCullough, and H. B. Gilbody, *J. Phys.* **B 8**, 2968 (1975).
- ¹⁹F. Ebel and E. Salzbom, in *Abstracts of 13th International Conference on the Physics of Electronic and Atomic Collisions, Berlin, 1983*, edited by J. Eichler, W. Fritsch, I. V. Hertel, N. Stolterfoht, and U. Wille (North-Holland, Amsterdam, 1983), p. 491.
- ²⁰M. Barat, C. Kubach, J. Pommier, C. Reynaud, V. Sidis, and Vu Ngoe Tuan, in *Abstracts of the Sixth International Seminar on Ion-Atom Collisions*, edited by Y. Nakai, K. Ozawa, and H. Tawara (Tokai-Mura, Ibaragi, Japan, 1979), p. 129.
- ²¹T. Nagata, Y. O. Kamura, E. Katoh, and Y. Mukoyama, *Phys. Lett.* **81A**, 265 (1981).
- ²²R. N. Il'in, V. A. Oparin, E. S. Solov'ev, and N. V. Federenko, *Zh. Tech. Phys.* **36**, 1241 (1966) [*Sov. Phys.—Tech. Phys.* **11**, 921 (1967)].
- ²³R. A. Baragiola and E. R. Salvatelli, *Phys. Rev. A* **12**, 806 (1975).
- ²⁴T. J. Morgan and F. J. Erikson, *Phys. Rev. A* **19**, 1448 (1979).
- ²⁵K. Rinn, A. Müller, H. Eichenauer, and E. Salzbom, *Rev. Sci. Instrum.* **53**, 829, (1982).
- ²⁶R. R. Hultgren, P. D. Dlsai, D. T. Hawkins, M. Gleiser, K. K. Kelly, and D. D. Wagman, *Selected Values of Thermodynamic Properties of the Elements* (American Society for Metals, Cleveland, 1973).
- ²⁷A. N. Nesmeyanov, *Vapor Pressure of the Chemical Elements*, edited by R. Gary (Elsevier, Amsterdam; 1963), p. 163.
- ²⁸O. Auciello, E. V. Alonso, and R. A. Baragiola, *Phys. Rev. A* **13**, 985 (1976).